A Numerical Study of Flow Structure in Over-Expanded Rocket Nozzles

Koichi YONEZAWA *Yukinori YAMASHITA* *Yoshinobu TSUJIMOTO*
Graduate School of Engineering Science, Osaka University
1-3, Machikaneyama-cho, Toyonaka, Osaka, 560-8531, Japan
E-mail: yonezawa@me.es.osaka-u.ac.jp

Yasuhide WATANABE
Tanegashima Space Center, Japan Aerospace Exploration Agency

Kazuhiko YOKOTA
Graduate School of Engineering, Nagoya Institute of Technology

Keywords: Rocket Nozzle, CTP Nozzle, RSS, FSS, Parametric Study, CFD

Abstract

LE-7A is the main engine of the H-IIA launch vehicle. Under its development, the nozzle suffered from two troubles during startup and shutdown transients of the engine. One is a large side load, which damages the actuator of the nozzle, and the other is damage on regenerative cooling tubes due to high heat load. It has been considered that these problems are caused by a peculiar separation pattern called Restricted Shock Separation (RSS). RSS is observed in several rocket nozzles, for example, LE-7A nozzle, Vulcain nozzle and so on. Their contours are not conventional truncated perfect (TP) nozzle – LE-7A nozzle is a compressed truncated perfect (CTP) nozzle and Vulcain nozzle is a thrust optimized (TO) nozzle. Although it is believed that the occurrence of RSS is affected by the nozzle contour, the mechanisms are not clarified sufficiently yet.

In the present paper, a parametric numerical study is carried out to investigate the mechanisms of the occurrence of RSS in CTP nozzles during startup transient. The results show that RSS is caused by the adverse pressure gradient downstream of the Mach disk. The adverse pressure gradient is caused by the interaction of the pressure wave and Mach disk. The method to avoid the occurrence of RSS is also examined. A small step inside the nozzle affects the position of the separation point and prevents RSS. The result shows that the possibility that RSS can be suppressed by controlling the position of the separation point.

Nomenclature

Symbols

C	= compression factor of nozzle contour
ε	= area ratio of nozzle
h	= height of step
L	= distance from throat to nozzle exit
p	= pressure
r	= radius
T	= temperature
x	= distance from throat in axial direction

Superscript

$( )^*$	= normalized by radius of throat

Subscript

$( )_a$	= ambient
$( )_t$	= throat
$( )_e$	= nozzle exit
$( )_{01}$	= inlet total

Abbreviations

BP	= Base Perfect
CP	= Compressed Perfect
CTP	= Compressed Truncated Perfect
FSS	= Free Shock Separation
NPR	= Nozzle Pressure Ratio, p_{01}/p_a
RSS	= Restricted Shock Separation
TP	= Truncated Perfect
TO	= Thrust Optimized

Introduction

LE-7A engine was developed as a modified version of LE-7 engine to enhance the reliability and to reduce the manufacturing cost. A Compressed Truncated Perfect (CTP) nozzle[1] was newly adopted to reduce the length of nozzle. The CTP nozzle is designed by compressing the Truncated Perfect (TP) nozzle[2] in axial direction.

As a result of this modification, two problems occurred during startup and shutdown transients in engine test. One is a large side load and the other is a damage on the regenerative cooling tubes[3), 4)].

Many researchers have studied about them[5)-11)] and it has become clear that the flow separation inside the nozzle caused the problems. In the LE-7A nozzle, two types of the separation pattern occur. In the first type, the separated free jet does not reattach on the nozzle wall as shown in Fig. 1 (a). Such separation pattern is called Free Shock Separation (FSS). FSS is a normal separation pattern and occurs in almost all types of supersonic nozzle under over-expanded conditions. In the other pattern, the

separated jet reattaches on the nozzle wall as shown in Fig. 1 (b). This separation pattern is called Restricted Shock Separation (RSS). RSS is a peculiar pattern and it is observed in the CTP nozzle, the Thrust Optimized (TO) nozzle and so on under a certain nozzle pressure ratio (NPR). A large side load occurs when the separation pattern changes between FSS and RSS. RSS also causes the heat load on the nozzle wall. When RSS occurs, shock wave is generated in the reattached supersonic jet and a high temperature region appears.

According to these facts, it is important for the development of the rocket nozzles to predict and avoid the occurrence of RSS. Although the mechanisms of the nozzle problems have become clear as mentioned above, the mechanisms and conditions of the occurrence of RSS are not clarified sufficiently. In the present paper, to clarify them, parametric numerical simulations are conducted. Computations are made for the startup transient of CTP nozzles with various contour. The effects of the contour compression factor and the amount of the truncation of the contour are investigated. We also try to suppress the occurrence of RSS by providing a step inside the nozzle.

Computational Overview

Numerical Procedure

In the present study, the flow field is assumed to be axisymmetric. The governing equations are compressible Navier-Stokes Equations. The flow field is assumed fully turbulent and the Spalart-Allmaras one equation turbulence model[12] is employed in the computation. The working fluid is air and treated as an ideal gas. The CFD code is based on the finite difference method. The accuracy in time and space are both second orders. The convective term is discretized by the AUSMDV[13] scheme with a second order upwind biased MUSCL interpolation. The viscous term is discretized by a central difference scheme. The time integration is made by the three-point-backward differencing scheme. The implicit relaxation with the LU-SGS[14] sub-iteration is used at each time step. The time step is 2.0×10^{-6} seconds.

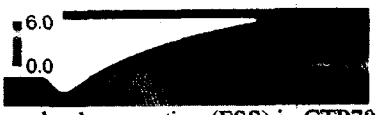

(a) Free shock separation (FSS) in CTP70S

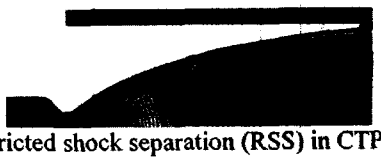

(b) Restricted shock separation (RSS) in CTP70L

Fig. 1 Separation patterns in CTP nozzles (NPR=25.0, Steady computation)

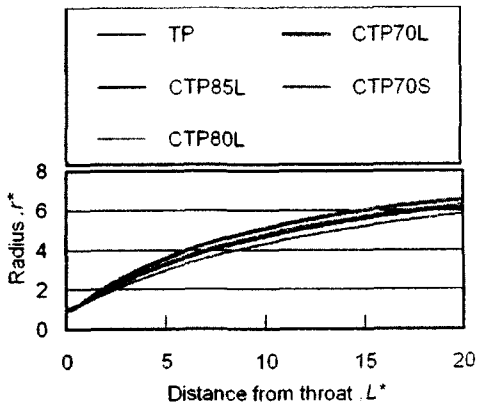

(a) Without step

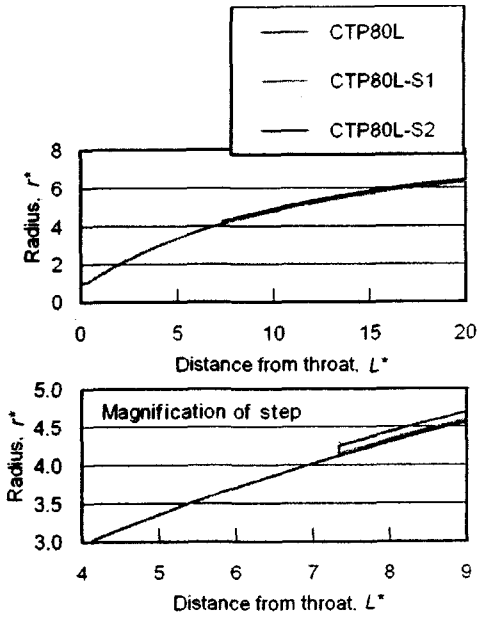

(b) With step

Fig. 2 Nozzle contours in diverging region

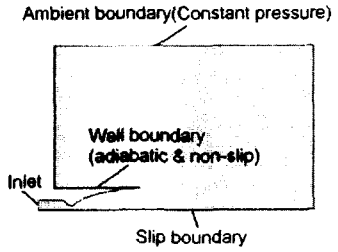

(a) Schematic of computational domain

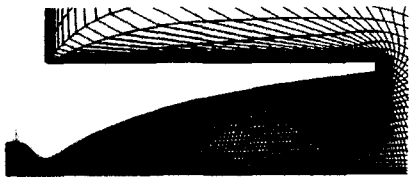

(b) Computational grid (around nozzle)

Fig. 3 Computational domain

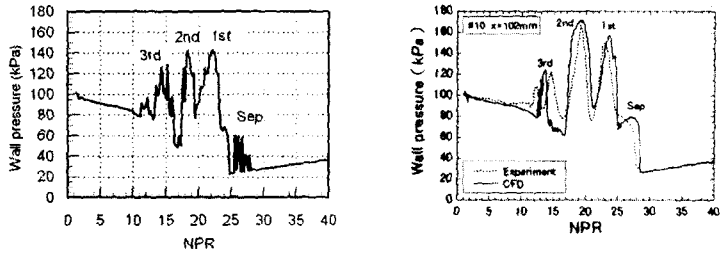

(a) x=102 mm

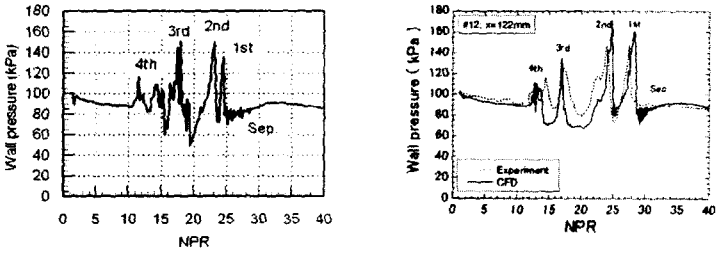

(b) x=122 mm

Fig. 4 Wall pressure versus NPR (Left; Numerical result, Right; Experimental and numerical result by Ref. 5), x=0mm; throat, x=124mm; nozzle exit)

Table 1 Configurations of computational nozzles

Contour	L^*	C(%)	ε	h^*
Base perfect	49	-	49	-
TP	20	100	34.8	-
CTP85L	20	85	38.4	-
CTP80L	20	80	39.7	-
CTP80L-S1	20	80	39.7	0.033
CTP80L-S2	20	80	41.0	0.133
CTP70L	20	70	42.3	-
CTP70S	13.3	70	32.5	-

Table 2 Grid for parametric computations

	Inside nozzle	Ambient region	Total
CTP50-R5-L	450 × 150	110 × 150	84000
CTP70S	320 × 100	100 × 100	42000
TP CTP70L CTP85L	370 × 100	130 × 100	50000
CTP80L	450 × 150	150 × 150	90000
CTP80L-S1 CTP80L-S2	520 × 150	130 × 150	97500

Table 3 Inlet condition

Contour	p_{01} [MPa]	Rate of increase [MPa/s]	T_{01} [K]	Rate of increase [K/s]
CTP50-R5-L	0.1-4.0	19.5	300	-
Other nozzles	0.1-12.0	7.93	300-3300	60000

Nozzle Configuration

We designed the TP and several CTP nozzles to investigate the effect of the amount of the contour truncation and the contour compression factor on the occurrence of RSS. Fig. 2 and Table 1 show their contour and geometric parameters, respectively.

Nozzles were designed by the following procedure.

i) First, a base perfect (BP) nozzle contour with a flat exit velocity distribution was designed by the method of characteristics. In the present work, the base perfect nozzle has the throat radius $r_t = 150$ mm, area ratio $\varepsilon = 49.0$ and the non-dimensional length between the throat and the nozzle exit $L^* = 49.0$. The throat radius is kept to be the same for all computations.

ii) A compressed perfect nozzle contour was generated from BP nozzle contour following:

$$C = \frac{\textit{Axial location of CP nozzle contour from throat}}{\textit{Axial location of BP nozzle contour from throat}} \times 100\,(\%) \quad (1)$$

Eq (1) indicates that the amount of contour compression becomes larger as the compression factor C decreases.

iii) The compressed perfect contour was truncated to obtain the CTP contour with certain L^*.

As the first step, we investigated the effects of the amount of the contour truncation by simulating for two 70% CTP nozzles – the CTP70L nozzle and the CTP70S nozzle. For these names, "70" indicates that $C = 70(\%)$, "L" indicates "longer ($L^* = 20$)" and "S" indicates "shorter ($L^* = 13.3$)."

As the second step, to investigate the effects of C, four types of nozzles were examined – the TP

nozzle, the CTP70L, 80% CTP nozzle (CTP80L) and 85% CTP nozzle (CTP85L), respectively. These nozzles have the length $L^* = 20$.

In the final step, we investigated the effect of the small step inside the nozzle on the suppression RSS. For this purpose, two types of nozzles are examined – the CTP80L-S1 and CTP80L-S2. Their base contour is the CTP80L and we provided the small step on the wall at the axial location of 37% L^* as shown in Fig. 2 (b). The axial positions of the step in two nozzles are the same but the step height of CTP80L-S1 is smaller than that of CTP80L-S2.

Computational Domain and Grid

The computational domain consists of the regions inside and outside the nozzle. Figure 3 shows schematic of the computational domain and the grid. The total length of the domain in the axial direction is about $8L^*$ from the throat to the nozzle exit. The length in the radial direction is about $5r_c$ from the axis. The number of the grid node is shown in Table 2.

Boundary and Initial Conditions

As an initial condition, it is assumed that the fluid in whole computational domain is stationary and the pressure and temperature are assumed to be 0.1MPa and 300K, respectively.

At the inlet boundary, the total pressure and the total temperature are fixed and the velocity is calculated by extrapolating the Riemann invariant from next grid node. The inlet total pressure and temperature are shown in Table 3. At the ambient boundary, the static pressure is fixed at 0.1MPa. The nozzle wall is treated as a non-slip and adiabatic wall.

Code Validation

First of all, the CFD code was validated through the comparison with experimental results[5), 6)] on CTP-50-R5-L nozzle. The present results are shown on the left hand side. The experimental and numerical results in Ref. 5) and 6) are shown on the right hand side. The results show several peaks of the pressure on each measuring point. Although the peak values of numerical result are slightly smaller, the NPRs that the peaks occur agree with each other. From these results, we consider that our CFD code can predict the unsteady nozzle flows qualitatively and quantitatively.

Results and Discussion

Effects of Truncation

As a first step, we examine the effect of the amount of truncation by comparing the results with CTP70L and CTP70S.

Figure 5 shows the Mach number distribution with instantaneous streamlines (upper) and pressure distribution (lower) of CTP70L nozzle during startup transient. At the NPR of 24.8 shown in Fig. 5 (a), the separation pattern is FSS and the streamlines downstream of Mach disk are almost parallel to the axis. Note that the pressure gradient downstream of the Mach disk is positive in this figure. At the NPR of 27.2 shown in Fig. 5 (b), a vortex ring appears at the nozzle exit. We considered that this vortex is caused by the pressure loss at the Mach disk and the adverse total pressure gradient. Due to this vortex, the pressure downstream the vortex and adverse pressure gradient become larger. The vortex pushes the separated supersonic jet to the nozzle wall as shown in Fig. 5 (c). Finally, the supersonic jet reattaches on the nozzle wall and result in RSS as shown in Fig. 5 (d). Under RSS, the separation region becomes small and the recirculation region appears in it. In Fig. 5 (e), the separation pattern recovered to FSS.

Fig. 6 shows the results with CTP70S nozzle. In CTP70S, the separation pattern is always FSS during startup transient. The vortex at nozzle exit does not occur while the Mach disk stays inside the nozzle.

Figure 7 shows the pressure distribution along the central axis. For CTP70L nozzle, the pressure behind the Mach disk is lower than the ambient pressure and increases in the axial direction. It is considered that the vortex in Fig. 5 is associate with this adverse pressure gradient. For CTP70S without the adverse pressure gradient, the vortex and RSS do not occur.

The above results show that RSS occurs in the longer nozzle with the smaller truncation.

Effects of Nozzle Contour Compression Factor

As the second step, we investigate the effect of the compression factor, C defined by Eq. (1). It is empirically known that RSS is favored by nozzles with smaller compression factor. However, quantitative relations between the compression factor C and the separation pattern have not been made clear.

Figure 8 shows the typical flow fields at the same NPRs in the CTP70L, CTP85L and TP nozzle, respectively. RSS occurs only in the CTP70L nozzle. In the CTP70L nozzle shown in Fig. 8 (a), we can see the adverse pressure gradient as mentioned in Fig. 5. In the CTP85L nozzle shown in Fig. 8 (b), the pressure behind the Mach disk is higher than that in the CTP70L nozzle. That is, the adverse pressure gradient is smaller for the CTP nozzle with larger compression factor (with small amount of the compression). In the TP nozzle shown in Fig. 8 (c), the pressure downstream of the Mach disk is higher than the ambient pressure and the pressure gradient is negative in axial direction. These results also show that the occurrence of RSS relates to the adverse pressure gradient inside the nozzle. Detailed examination of the result shows that differences are caused by the difference of the pressure wave in nozzle. In the diverging region of the supersonic nozzles, the compression waves are generated in the vicinity of the throat. These waves produce the internal shock as shown in the figures. These internal shocks enclose the a high-speed region called "kernel." As C becomes smaller, the kernel becomes larger and closing point shifts downstream. In the TP nozzle, the kernel is the smallest in the

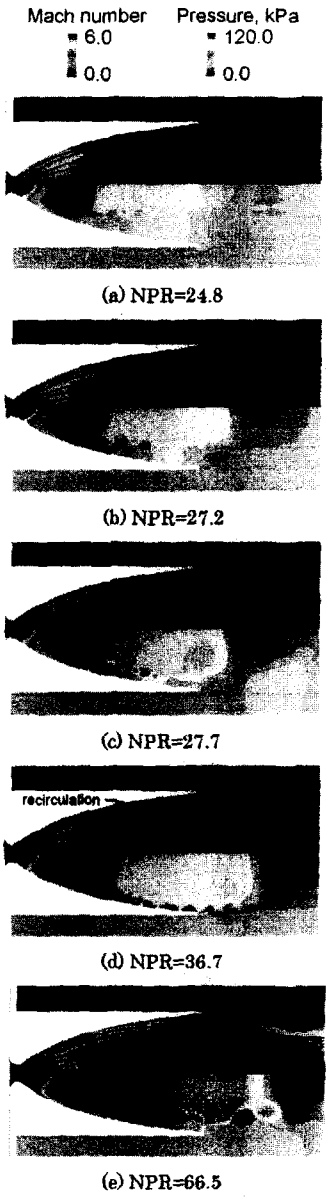

Fig. 5 Mach number field with instantaneous streamlines (upper) and pressure distribution (lower) (startup of CTP70L nozzle)

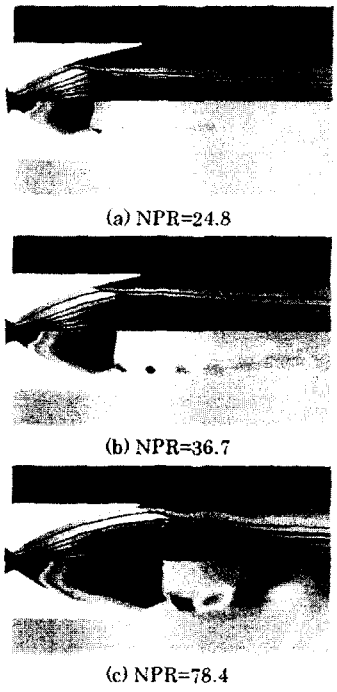

Fig. 6 Mach number field with streamlines(top) and pressure distribution(bottom) (startup of CTP70S nozzle)

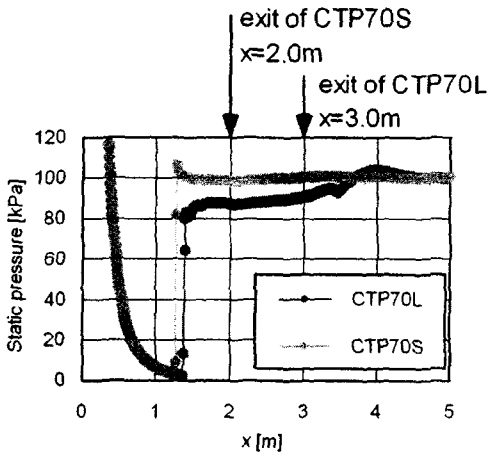

Fig. 7 Pressure distribution on central axis in CTP70L and CTP70S nozzle (NPR=24.8)

three and the Mach disk appears at the downstream of the closing point of the kernel as shown in Fig. 8(c). On the other hand, in CTP nozzles as shown in Fig. 8 (a) and (b), the Mach disk appears upstream of the closing point of the kernel. In addition, because the Mach number just upstream of the Mach disk is the highest in CTP70L, the pressure loss is also the highest. Therefore, the pressure downstream of the Mach disk becomes the lowest.

Figure 9 shows the typical flow fields during startup of the CTP80L nozzle. Figure 9 (a) and (b) show the flow field before and after the transition from FSS to RSS. Under RSS, axial location of the separation point is closer to the nozzle exit than the Mach disk. Figure 9 (c) and (d) shows the transition from RSS to FSS. At the condition of Fig, 9 (c), the separation point reaches the nozzle exit. As the NPR becomes larger, the separation pattern recovers to FSS and the separation point shifts upstream. Comparing with the CTP70L nozzle shown in Fig. 5, the amount of the shift is obviously larger.

Figure 10 shows the axial position of the shock and the separation point versus the NPR for CTP85L, CTP80L, CTP70L and CTP50-R5-L[5), 6)] (50% CTP nozzle), respectively. In the CTP85L nozzle, because

RSS does not occur, both positions changes smoothly. On the other hand, in the CTP80L nozzle, the rapid movement of the shock and separation point occurs at the transition between FSS and RSS. This can be seen also for CTP70L and the CTP50-R5-L nozzle. However, the movement of the separation point is significantly larger for CTP80L nozzle.

Suppression of RSS by a step inside nozzle

The transition to RSS may cause a large side load and high heat transfer to nozzle wall. Therefore the suppression of it is quite important. The simplest suppression method is to adopt the TP nozzle. In TP nozzles, RSS does not occur though there are some exceptions. However, the TP nozzle has some demerits. For example, it has long contour due to the design method. In this section, we try to suppress RSS by providing the small step in a CTP nozzle.

Figure 11 shows the axial locations of the separation point for CTP80L, CTP80L-S1 and CTP80L-S2. For CTP80L the separation point shifts quite downstream between the NPR of about 30 and about 50. For CTP80L-S1 nozzle with a smaller step, the range of the NPR with RSS is smaller than that in CTP80L nozzle. In the CTP80L-S2 nozzle with a larger step, RSS does not occur. This shows that RSS can be suppressed by the step. Although the step can avoid RSS, this method has also a problem. That is, the rapid movement of separation point when it passes the step can cause the serious side load. However, these result show the possibility that RSS can be suppressed by controlling the position of the separation point by using the step.

Conclusion

In the present paper, we conducted a series of numerical investigations for the CTP nozzles to clarify the mechanisms of the occurrence of RSS. The results can be summarized as follows:

- RSS is associated with the adverse pressure gradient downstream of the Mach disk inside the nozzle.
- The pressure gradient downstream of the Mach disk inside the nozzle is affected by the amount of the truncation of the nozzle contour. The adverse pressure gradient and RSS occur in the long nozzles with small truncation.
- The pressure gradient downstream of the Mach disk inside the nozzle is affected by the compression factor of the nozzle contour. In the nozzle with high compression factor, the kernel becomes large and results in the generation of the adverse pressure gradient.

In addition, a suppression method of RSS was examined by providing a small step inside the nozzle. The results show the possibility that RSS can be suppressed by controlling the position of the separation point.

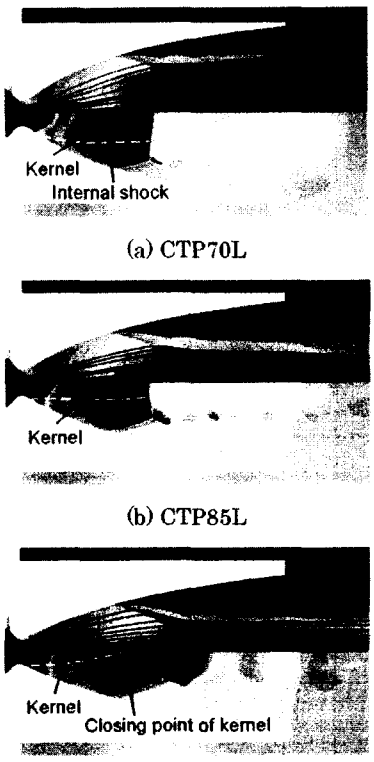

(a) CTP70L

(b) CTP85L

(c) TP

Fig. 8 Mach number field with instantaneous streamlines (upper) and pressure distribution (lower) (NPR=27.2, Startup of CTP70L, CTP85L and TP nozzle)

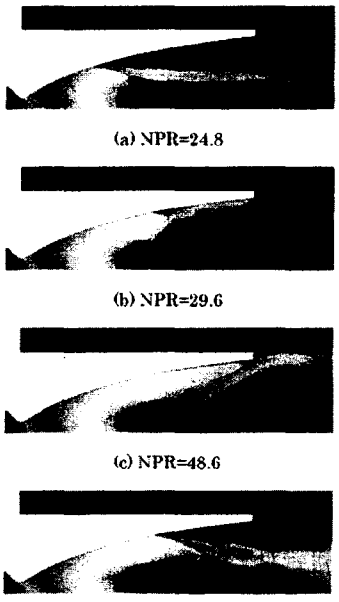

(a) NPR=24.8

(b) NPR=29.6

(c) NPR=48.6

(d) NPR=52.17

Fig. 9 Mach number field (startup of CTP80L nozzle)

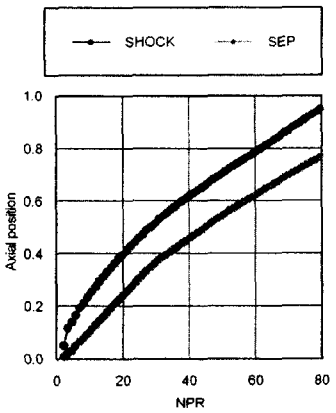

(a) CTP85L

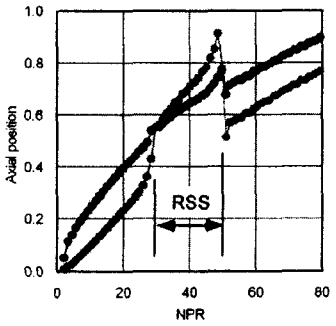

(b) CTP80L

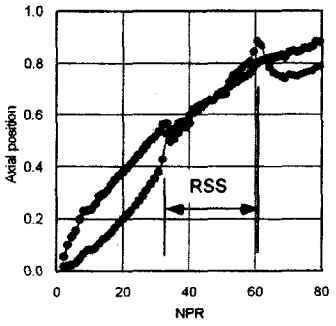

(c) CTP70L

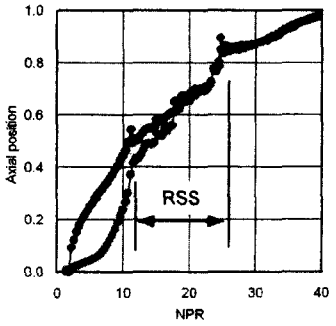

(d) CTP50-R5-L

Fig. 10 Axial position of Mach disk on central axis and separation line on nozzle wall (startup of CTP85L, CTP80L, CTP70L and CTP50-R5-L nozzle)

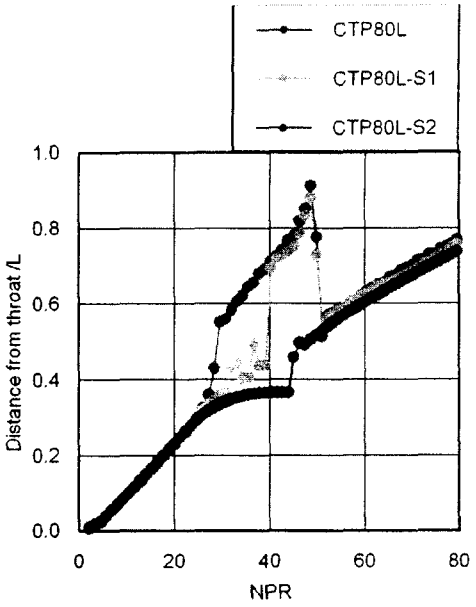

Fig. 11 Axial position of separation line (startup of CTP80L, CTP80L-S1, CTP80L-S2)

Acknowledgement

The present work was supported by National Aerospace Laboratory (currently Japan Aerospace Exploration Agency).

References

1) Hoffman, J. D., "Design of Compressed Truncated Perfect Nozzles," AIAA-85-1172, 1985
2) Ahlberg, J. H., et al, "Truncated Perfect Nozzles in Optimum Nozzle Design," ARS Journal, May 1961, pp. 614-620
3) Watanabe, Y., et al, "LE-7A Engine Nozzle Problems During the Transient Operations," AIAA-2002-3841, 2002
4) Watanabe, Y., et al, "LE-7A Engine Separation Phenomenon Differences of the Two Nozzles Configurations," AIAA-2003-4763, 2003
5) Takahashi, M. et al, "Transient Flow Simulation of a Compressed Truncated Perfect Nozzle," AIAA-2001-3681, 2001
6) Tomita, T., et al, Visualization of the Formation of Separation Bubbles on a Bell-Shaped nozzle Surface in Relation to Serious Side-Load," AIAA-2001-3559, 2001
7) Gross, A., et al, "Experimental and Numerical Investigation of Heat Loads in Separated Nozzle Flow," AIAA-2001-3682, 2001
8) Frey, M. and Hagemann, G., "Restricted Shock Separation in Rocket Nozzles," Journal of Propulsion and Power, Vol. 16, No. 3, pp. 478-484, 2000
9) Hagemann, G. and Frey, M., "Appearance of

Restricted Shock Separation in Rocket Nozzles," Journal of Propulsion and Power, Vol. 18, No. 3, pp. 577-584, 2002
10) Tomita, T., et al, "Sub-Scale Nozzle Combustion Tests of the LE-7A Engines for Clarification of Large Side-Loads (I)," AIAA-2002-3842, 2002
11) Tomita, T., et al, "Sub-Scale Nozzle Combustion Tests of the LE-7A Engines for Clarification of Large Side-Loads (II)," AIAA-2002-4002, 2002
12) Spalart, P. R. and Allmaras, S. R., "A One-Equation Turbulence Model for Aerodynamics Flows," La Recherche Aerospatiale, No. 1, pp. 5-21, 1994
13) Wada, Y. and Liou, M. –S., "An Accurate and Robust Flux Splitting Scheme for Shock and Contact Discontinuities," SIAM Journal on Scientific Computing, Vol. 18, No. 3, pp. 633-657, 1997
14) Jameson, A., and Yoon, S., "Lower-Upper Implicit Schemes with Multiple Grids for the Euler Equations," AIAA Journal, Vol. 25, No. 1, 1987, pp. 929-935